Cite this article
Arnold A, Portmann G and Li Q (2026)
Centrifuge tests on the load-bearing behaviour of prefabricated concrete screw-type piles.
International Journal of Physical Modelling in Geotechnics **26(2)**: 105–117,
https://doi.org/10.1680/jphmg.25.00036

Research Article
Paper 2500036
Received 29/11/2023; Accepted 28/10/2025

International Journal of Physical Modelling in Geotechnics

Centrifuge tests on the load-bearing behaviour of prefabricated concrete screw-type piles

André Arnold
Institute of Civil Engineering, Lucerne University of Applied Sciences and Arts, Horw, Switzerland (Orcid:0009-0006-0653-5518) (corresponding author: andre.arnold@hslu.ch)

Gregor Portmann
Institute of Civil Engineering, Lucerne University of Applied Sciences and Arts, Horw, Switzerland (Orcid:0009-0004-0635-9521)

Qiang Li
PowerChina Huadong Engineering (Shenzhen) Corporation Limited, Shenzhen, China; Faculty of Civil Engineering and Geosciences, Delft University of Technology, Delft, The Netherlands (Orcid:0009-0001-7588-3819)

Due to very low noise emission during installation, prefabricated concrete screw-type piles (PCSP) could potentially be viable options as foundations for offshore and onshore structures. However, little attention has been paid to the axial load-bearing behaviour in compression of this specific prefabricated screw-type pile system in comparison with conventional displacement pile systems. This article describes an experimental campaign of centrifuge tests performed at 100*g* on both screw-type piles and straight shafted piles (SP) with diameters of 550 and 475 mm at prototype scale. The outer screw diameter (D_s) to pile core diameter (D) ratio amounted to $D_s/D = 1.25$, and the screw pitch (L_p) to pile core diameter (D) ratio (pitch ratio) was selected as $L_p/D = 0.57$. Saturated *Vingerling Clay* was used to model the soil layer, and a low loading rate was selected to simulate drained conditions. Piles were installed at 1*g*; therefore, the pile installation process was not fully modelled. For both pile diameters investigated, the results indicate an approximately 45% higher bearing capacity with the PCSP compared with the capacity of the SP.

Keywords: centrifuge modelling/foundations/geotechnical engineering/piles and piling/soil structure interaction

Notation

AR	advancement ratio
CD	consolidated, drained (for triaxial testing)
c_v	consolidation coefficient
D	pile core diameter (identical to outer diameter for straight shafted piles)
D_s	outer screw diameter
d	length of drainage path
e	void ratio
e_0	initial void ratio
g	Earth's gravitational acceleration
h_R	helical rib height
h_0	initial height of triaxial probe
I_p	plasticity index
K	lateral earth pressure coefficient
K_0	lateral earth pressure coefficient at rest
k	hydraulic conductivity
L	pile length
L_0	embedded length of the pile
L_p	screw pitch
M_E	soil stiffness from an oedometer test (normal compression line) $M_E = \Delta\sigma'/\Delta\varepsilon$
M'_E	soil stiffness from an oedometer test (unloading-reloading line) $M'_E = \Delta\sigma'/\Delta\varepsilon$
NCL	normal compression line
OCR	over consolidation ratio
PCSP	prefabricated concrete screw-type pile
Q	axial pile load
Q_b	base resistance
Q_s	shaft friction
q_m	shaft friction at ultimate limit state
R_t	roughness depth
S_r	degree of saturation
SP	straight shafted pile
s	settlement
s_u	undrained shear strength
$s_{u,crit}$	undrained shear strength at critical state
$s_{u,max}$	peak undrained shear strength
T_v	time factor for one-dimensional consolidation
t	time
U_m	coefficient of consolidation
ULS	ultimate limit state
URL	unloading-reloading line
USCS	unified soil classification system
V	normalised velocity
v	settlement rate
w	in-situ water content
w_L	liquid limit
w_P	plastic limit
Δa	axial displacement in triaxial tests
α_H	helix angle
β	drained interface strength parameter
γ	unit weight of soil
γ_d	dry unit weight of soil

γ_s	unit weight of solid particles
γ_w	unit weight of water
δ'	angle of friction between pile and soil
σ'_h	horizontal effective stress
σ'_{v_0}	mean vertical effective stress
σ'_z	effective normal stress in an oedometer test
σ'_0	effective preconsolidation stress from an oedometer test
τ_{int}	interface shear strength
φ'	friction angle
φ'_{crit}	friction angle at critical state
φ'_{max}	peak friction angle

1. Introduction

A new prefabricated concrete screw-type pile (PCSP) system has been developed (details given in Table 1 and Figure 1) and employed for a wide range of applications, such as pile foundations for masonry buildings and nearshore test foundations for the feasibility studies of a cable car project across Lake Zurich (Arnold *et al*., 2021). This system offers several advantages over conventional cast-in-place pile systems:

Table 1. Details on the PCSP geometry

Geometry details	Larger PCSP	Smaller PCSP
Outer screw diameter D_s	550 mm	475 mm
Pile core diameter D	440 mm	365 mm
Screw pitch L_p	250 mm	250 mm
Helix angle α_H	30°	30°
Helical rib height h_R	55 mm	55 mm
D_s/D	1.25	1.30
L_p/D_s	0.45	0.53

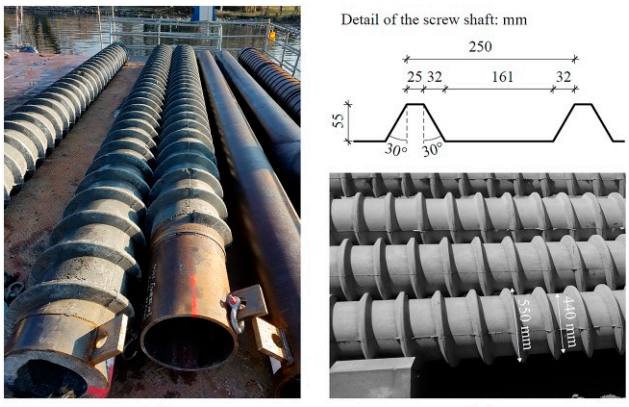

Figure 1. Prefabricated concrete screw-type piles (PCSP) for the test foundation of the cable car project across Lake Zurich. (a) Prefabricated concrete screw-type piles (Arnold and Askarinejad, 2020); (b) general information on PCSP geometry

- Prefabricated piles have constant cross-sections; hence, there is no risk of cross-sectional narrowing due to local soil failure within the drilled hole.
- There is no possibility of a hydraulic fracture forming at the base of the pile during installation since the pile system is close-ended.
- The screw-type geometry provides a rough pile shaft surface, which leads to a potentially enhanced load-bearing behaviour compared with the widely used straight shafted concrete piles.

The screw blades are uniformly distributed along the total embedded length of the pile.

1.1 Aim of centrifuge tests

The aim of centrifuge tests is to enable a direct comparison of the load-bearing behaviour of this specific PCSP to that of commonly used straight shafted piles (SP) with equal diameter in the same soil layer. The focus is to demonstrate possible advantages of this specific screw geometry over a straight shafted system by means of physical models. The geometry of the PCSP has already been determined at an earlier stage. The physical model tests, therefore, serve to analyse the load-bearing behaviour of the given PCSP.

1.2 Background

Several studies have been conducted on steel screw piles with helical form and a discrete number of blades (generally <5) for offshore and onshore applications (e.g. Byrne and Houlsby, 2015; Davidson *et al*., 2022; Knappett *et al*., 2014; Nabizadeh and Choobbasti, 2017). Generally, the ratio of the outer screw diameter to pile core diameter (D_s/D) ranges between 2 and 4.

Hird and Stanier (2010) observed cylindrical failure surfaces in their tests on single- and triple-helix piles (helix diameter: D_s = 20 mm; pile diameter: D = 5 mm; L_p/D_s = 1.5 or 3; D_s/D = 4.0) installed in synthetic transparent soil (screwed into a clay analogue at constant screw rate). The observed cylindrical shear bands are formed more clearly with the use of a triple-helix pile. Furthermore, their results indicate that the triple-helix pile provided an approximate axial bearing capacity of 130 N, which is an improvement compared with the axial bearing capacity of the single-helix pile, with approximately 70 N.

Byrne and Houlsby (2015) showed failure mechanisms of helical screw piles with two blades in clay and sandy soils. They concluded that an envelope friction with a virtual pile diameter equal to the blade diameter might be considered. Furthermore, Knappett *et al*. (2014) showed that the bearing capacity of screw piles with a discrete number of blades in sandy soil is substantially higher than that of SP.

Meng *et al*. (2017) conducted both numerical investigations and small-scale physical model tests to study the load-bearing behaviour of drilled displacement piles with uniformly distributed screw

blades along the pile shaft in sandy soil. In the numerical model, the piles, which were modelled as 'wished in place', had a length of 15 m, a core diameter (D) of 0.370 m, and an outer screw diameter (D_s) of 0.550 m, giving a D_s/D ratio of 1.49. The cross-sectional dimensions are comparable with those of the PCSP (Figure 1), although D_s/D is slightly higher. The soil was simulated using an elastic-perfectly plastic model, employing a Mohr–Coulomb failure criterion. Results of their numerical simulations, depicted in Figure 2, qualitatively illustrate the plastic zones surrounding the screw threads at the ultimate limit state (ULS). Contrastingly, the numerical simulations for piles with a straight shaft revealed no plastic zone in the surrounding soil. The size of the plastic zone was found to depend on the screw pitch (L_p). A smaller L_p ranging from 250 mm (L_p/D = 0.68) to 500 mm (L_p/D = 1.35) led to the formation of a continuous plastic zone, whereas a larger L_p (750–1000 mm) resulted in discontinuities in the resulting plastic zone. This suggests a strong correlation between screw pitch ratio and bearing capacity of the pile. However, it is important to note that the size and shape of plastic zones derived from numerical models are influenced by the finite-element mesh size and the constitutive model used for the soil. Consequently, the results should be viewed as qualitative indications of the effect of screw pitch ratio on local pile–soil interaction. Approximate values of bearing capacities using the slope tangent method after O'Rourke and Kulhawy (1984), derived from the diagrams in Meng *et al*. (2017), are provided in Table 2.

Both the contributions of Meng *et al*. (2017) and Hird and Stanier (2010) showed plastic zones around the screw piles, which indicate that shear strength due to axial pile loading is mobilised directly in the soil and not on the pile–soil interface, as results with SP.

Gorasia (2013) conducted centrifuge model tests at 50g to study the behaviour of ribbed piles (piles bored and cast at 1g; pile core diameter D = 16 mm; outer rib diameter D_s = 19 mm; pile length L = 180 mm) in overconsolidated, artificially produced kaolin clay. The tests showed that the use of ribs was found to always increase the bearing capacity compared with SP (D = 16 mm). It was also concluded that the helically ribbed profile with D_s/D = 1.19 and L_p/D_s = 0.53 was shown to be the most effective of all tested profiles. Of main interest for the herein presented model tests are the load-settlement curves Gorasia (2013) shows for ribbed piles compared with SP. It can be observed that the SP shows a similar increase in load for low settlements compared with ribbed piles. With larger pile settlements, the ribbed pile shows a higher bearing capacity than the SP, whereas the SP seem to show a decrease in axial load with larger pile settlements.

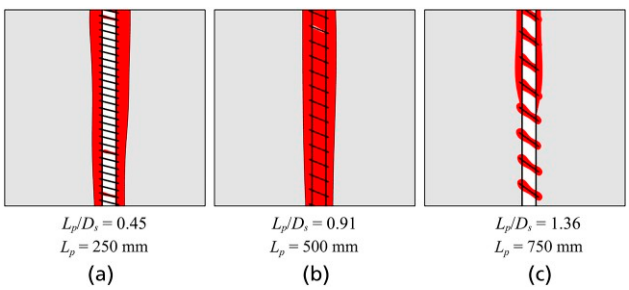

Figure 2. Numerical model after Meng *et al*. (© 2017; reproduced with permission of the licensor through PLSclear) to qualitatively show the plastic zones (indicated in red) at ULS as a function of L_p: screw piles with D = 370 mm, D_s = 550 mm and (a) L_p = 250 mm, (b) 500 mm and (c) 750 mm

Table 2. Approximate bearing capacity for the piles given in Figure 2 (Meng *et al*., 2017)

Pile D_s/D = 1.49	Approximate bearing capacity in terms of axial load: kN	Normalised bearing capacity in terms of axial load
Straight shafted pile	1000	1
L_p/D = 0.68; L_p = 250 mm	2300	2.3
L_p/D = 1.35; L_p = 500 mm	2000	2
L_p/D = 2.03; L_p = 750 mm	1600	1.6

Gorasia and McNamara (2015) describe their centrifuge model tests on the load-bearing behaviour of ribbed piles compared with SP in the same soil layer. They constructed the piles at 1g conditions and tested the piles in the centrifuge (at 50g). Their results show that the normalised bearing capacity (normalised to the SP) decreases with increasing rib spacing, which can be compared with the findings given by Meng *et al*. (2017).

1.3 General load-bearing behaviour of axially loaded piles

The general load-bearing behaviour of piles is summarised to correctly interpret the test results (Figure 3). Kempfert (2009) proposed a normalised settlement of s/D = 0.1 to mobilise the bearing

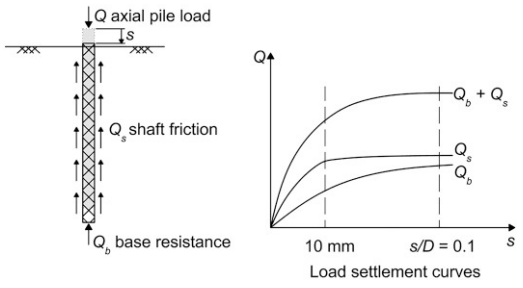

Figure 3. General load-bearing behaviour of piles after Atkinson (© 2007; reproduced by permission of Taylor & Francis Group), indicating the mobilisation of base resistance and shaft friction

capacity for all kinds of soils. Franke (1982) proposed a normalised settlement of $s/D = 0.1...3.0$ for the development of full base resistance in sandy soil and 0.05...2.0 for clay, whereas the shaft resistance could be mobilised with a settlement of 20 mm in sandy soils and 10 mm in clay. It is generally observed that the base resistance Q_b (Figure 3) increases steadily up to the bearing capacity and can be improved by increasing pile penetration. The shaft friction Q_s (Figure 3), however, is already fully mobilised after small settlements and remains approximately constant for further pile penetration.

2. Centrifuge model tests on PCSP

Model tests were carried out using the geotechnical centrifuge at Delft University of Technology (Allersma, 1994; Li *et al*., 2020) to study the axial compressive load-bearing behaviour of the PCSP at an acceleration of 100*g*. The installation effects were, however, not investigated. The centrifuge tests were conducted in saturated clay under drained conditions, as the PCSP are typically employed to bear permanent loads. Furthermore, the centrifuge tests were conducted under strain-controlled conditions.

The piles had an outer screw diameter D_s of 475 and 550 mm, respectively, at prototype scale, resulting in an outer diameter of 4.75 and 5.5 mm, respectively, at model scale.

2.1 Soil properties and model preparation

Each centrifuge model consisted of two piles, one PCSP model and one SP model in clay (Figure 4(a)). The PCSP models were manufactured using a three-dimensional (3-D) metal printer and exhibited the same geometry as the prototype piles, including the pile tip (Figure 5). The SP had the same outer diameter (D = 5.5 mm), length, and the same tip as the PCSP model (D_s = 5.5 mm, D = 4.4 mm; L_p = 2.5 mm). The only difference being that these piles had a straight shaft consisting of aluminium with a certain roughness caused by the 3-D printing process. Pile stiffness and strength were not compared with the concrete prototype. However, the prototype pile was considered to be stiff in relation to the soft clay soil. The surface roughness (e.g. Fioravante, 2002; Tolun *et al*., 2023) of the SP model was measured in terms of roughness depth R_t and compared with concrete surfaces available in the lab (Table 3) as well as with investigations on pile roughness (Table 4) by Tolun *et al*. (2023).

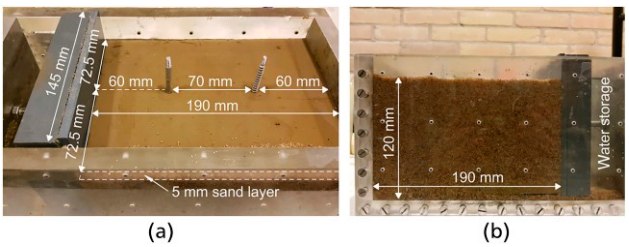

Figure 4. (a) Model piles in clay soil; (b) soil model with sand layer and water storage

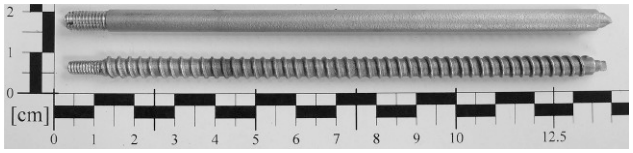

Figure 5. Model of the straight shafted pile and the screw-type pile; both piles had an embedment length $L_0 \approx 90$ mm

The roughness of the SP model was higher compared with a concrete surface produced with plastic formwork but comparable with ordinary produced mortar and also with steel and aluminium piles investigated by several authors (Tolun *et al*., 2023; Table 4). However, the roughness of prototype piles (straight shafted; installed as a displacement pile with cast-in-situ concrete) depends on the production method as well as on the adjacent soil type. The surface roughness of the PCSP was not directly measured, as the screw geometry assumingly has a greater influence on the interface behaviour than its surface roughness. However, as the PCSP was printed the same way as the SP, the surface roughness should be the same.

Blocks of *Vingerling Clay* K122 (Hiemstra and Rijsdijk, 2003), which is a naturally occurring clay sediment available in blocks, were used in the tests. The blocks were placed into the strongboxes (Figure 4) and subsequently flooded with water through the water storage. The water table in the water storage was set equal to the clay block height. The geotechnical properties of the natural material were obtained from laboratory tests using vane shear-,

Table 3. Surface roughness of different materials

Investigated surface	Roughness depth R_t: mm
Straight shafted model pile (3-D-printed aluminium)	0.0198
Concrete (produced with plastic formwork)	0.0046–0.0133
Mortar	0.0177–0.0283

Table 4. Surface roughness of different pile materials (after Tolun *et al*., 2023)

Investigated surface	Roughness depth R_t: mm
Fioravante (2002) (aluminium)	0.002–0.10
Jardine *et al*. (2013) (steel)	0.008
Lehane *et al*. (1993) (steel)	0.016

oedometer-, triaxial-, and direct shear tests (Table 5 and Figure 6). Vane shear tests were conducted after the centrifuge tests in undisturbed zones of the clay blocks. The soil parameters were subsequently used in the consolidation calculations as well as for analytical modelling.

The clay blocks were placed in the strongbox (inner geometry: 270 × 150 × 150 mm) with thin layers of fine sand underneath and on one of the side walls to ensure drainage to the water storage. This measure was to more accurately simulate drained soil conditions through shorter drainage paths to the ground floor and one side wall (Figure 4(b)). The clay blocks showed an overconsolidated behaviour during the pile load tests with an OCR of approximately 2.4 at $L_0/2$ (Figure 6(a)).

2.2 Installation of model piles in the soil

The model piles were either pressed into the soil (SP) or screwed (PCSP) manually with a constant penetration rate at 1*g*. The installation effects generally influence the loading behaviour of piles (Madabhushi, 2014). However, the focus of the tests described herein was to compare the load-bearing behaviour of SP to PCSP. Therefore, a simplified pile installation at 1*g* was accepted, as installation conditions were similar for both pile geometries. An installation tool was used (Figure 7) to ensure reproducible installation conditions at 1*g*, applying a pitch-matched installation (AR = 1.0) of the PCSP as described in Cerfontaine *et al*. (2021) to reduce soil disturbance during pile installation. The strongbox was finally covered with a plastic cover to prevent the model from drying out. Table 6 provides an overview of the

Table 5. Soil properties of *Vingerling Clay* K122 blocks

Soil property	Notation	Measured value
Water content	w	30.4%
Plastic limit	w_p	24.0%
Liquid limit	w_L	49.6%
Plasticity index	I_p	25.6%
USCS classification	—	CM
Initial void ratio	e_0	0.81
Unit weight of solid particles	γ_s	27.5 kN/m^3
Dry unit weight	γ_d	15.2 kN/m^3
Unit weight	γ	19.5 kN/m^3
Saturation degree	S_r	96%
Hydraulic conductivity*	k	$\approx 1 \cdot 10^{-9}$ m/s
Peak undrained shear strength in situ (Vane shear tests after centrifuge tests)	$s_{u,max}$	37 kN/m^2
Undrained shear strength at critical state (Vane shear tests after centrifuge tests)	$s_{u,crit}$	27 kN/m^2
Peak friction angle (direct shear test; vertical effective stress 100 kPa)	φ'_{max}	31.8°
Friction angle at critical state (direct shear test and triaxial CD test)	φ'_{crit}	24. . .26°
Pre-consolidation stress	σ'_0	≈ 100 kPa
Soil stiffness (normal compression line)	M_E	4000 kN/m^2
Soil stiffness (unloading–reloading line)	M'_E	12 000 kN/m^2

*The hydraulic conductivity k could not be measured directly and was assumed to be equal to 1×10^{-9} m/s

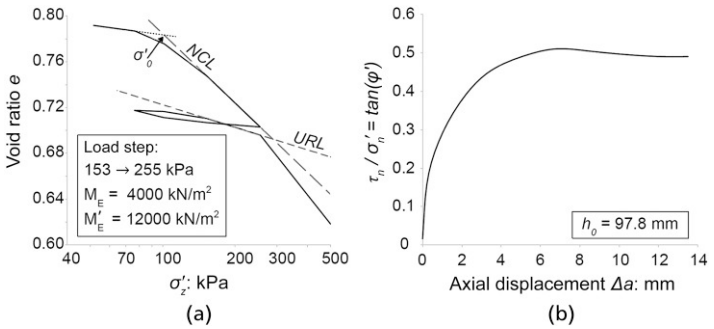

Figure 6. Laboratory testing of *Vingerling Clay* K122: (a) oedometer test with NCL, URL, $\sigma'_0 \approx 100$ kPa; (b) mobilised shear strength against axial displacement in a triaxial CD test (axial compression) with shear rate 0.001 mm/min

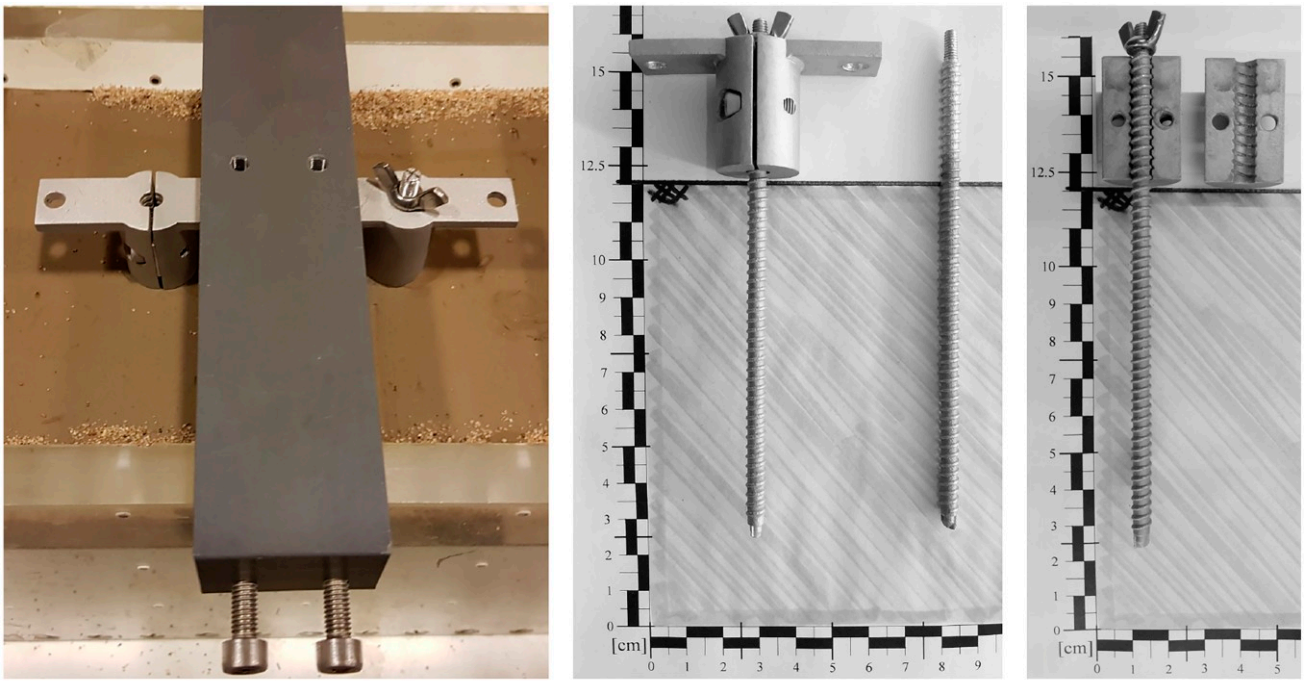

Figure 7. (a) Installation of the model piles at 1*g* with an installation tool; (b) and (c) detail view of the installation tool for PCSP

Table 6. Overview of installed piles and measured soil conditions. Pile diameter, embedded length, and penetration rate are given in prototype scale

Test name	Pile (outer) diameter	Embedded length	Penetration rate	Undrained shear strength (Vane shear tests) s_u: kN/m²		Water content
T	$D_{(s)}$: m	L_0: m	*v*: mm/s	$s_{u,max}$	$s_{u,crit}$	*w*: %
T1 (screw)	0.55	9.2	0.01	39	24.5	30.4
T2 (screw)	0.55	9.25	0.005	39	24.5	30.4
T3 (screw)	0.55	9.29	0.005	34	23.6	30.4
T4 (straight shafted)	0.55	9.34	0.005	34	23.6	30.4
T7 (screw)	0.475	9.5	0.005	37.7	28.6	30.4
T7r (screw)	0.475	9.4	0.005	36.3	28.1	30.3
T8 (straight shafted)	0.475	9.4	0.005	37.7	28.6	30.4
T8r (straight shafted)	0.475	9.3	0.005	36.3	28.1	30.3

installed piles, the penetration rates used, and the measured soil conditions. All piles had a distance of at least 4.5D to the bottom of the strongbox after installation. Hence, the influence of the base on the bearing capacity of the piles may be considered to be negligible (e.g. Lambe and Whitman, 1969; Lang *et al*., 2011).

2.3 Test procedure

The models were consolidated at 100*g* during a period of 40 min to obtain well-defined soil conditions in terms of consolidation (free water table in the water storage; water storage linked to the clay block by way of sand layers). A period of 40 min of consolidation in the centrifuge at 100*g* translates to a prototype consolidation duration of 278 days and leads to a consolidation degree U_m of approximately 89% using the one-dimensional (1-D) consolidation theory of Terzaghi (1943):

1. $$T_v = \frac{k \cdot t \cdot M_E}{d^2 \cdot \gamma_w}$$

Considering the parameters $k = 10^{-9}$ m/s, $t = 278$ days, and $M'_E = 12\,000\,\text{kN/m}^2$ (provided by the oedometer test for over-consolidated soil), a maximum drainage path of $d = 6$ m (assuming vertical, 1-D drainage; see Figure 4(b)) and $\gamma_w = 10\,\text{kN/m}^3$, T_v results in a value of 0.801. Finally, U_m is calculated using T_v and Equation 2 (e.g. Knappett and Craig, 2012):

2. $$T_v = -0.933 \cdot \log(1 - U_m) - 0.085 \; for \; U_m > 0.526$$

For values of $U_m < 10\%$, mainly undrained behaviour can be assumed, whereas for $U_m > 70\%$, the soil will have a drained behaviour (Wehnert, 2006, after Vermeer and Meier, 1998). With U_m amounted to approximately 89% after the consolidation, the clay blocks were assumed to have a drained behaviour at the onset of the pile loading tests according to Equations 1 and 2. U_m is even higher in the soil model. This assumption is based on the fact that the consolidation of the clay blocks was not exclusively 1-D (due to one side of the block being in contact with fine sand; see Figure 4(b)).

After consolidation, one of the two piles was tested axially at model scale. The pile was loaded at a constant penetration rate of 0.005 mm/s in accordance with the recommendation of Knappett and Craig (2012). The penetration rate is equal in model and prototype scale (Madabhushi, 2014; Wood, 2004). Garnier *et al.* (2007) suggested a normalised velocity V (after Kutter, 1994, and Randolph *et al.*, 2005) to investigate the transition between drained and fully undrained conditions in terms of loading rate:

3. $$V = \frac{v \cdot d}{c_v} = \frac{v \cdot d}{\frac{k \cdot M_E}{\gamma_w}} = \frac{0.005\,\frac{\text{mm}}{\text{s}} \cdot 5.5\,\text{mm}}{\frac{10^{-9}\,\text{m}}{\text{s}} \cdot 12000\,\text{kN/m}^2}{10\,\text{kN/m}^3} = 0.02\,[-]$$

with the parameter V equal to 0.01 for fully drained conditions and $V = 30$ for fully undrained conditions. A value of $V = 0.02$ indicates that the loading rate is low enough to maintain drained conditions. The centrifuge had to be stopped for a short period to install the load actuator for the second model pile. The centrifuge was subsequently accelerated again, and the model was consolidated at 100*g* during a further 5 min to ensure consolidated conditions for the second pile test (Figure 8).

3. Test results

3.1 Influence of the penetration rate

Two different penetration rates (rate v_{T1}: 0.01 mm/s, $V = 0.05$; rate v_{T2}: 0.005 mm/s, $V = 0.02$) were used on the model piles with $D_s = 5.5$ mm to investigate the influence of the penetration rate on the load-bearing behaviour. Tests T1 and T2, which were conducted using the same *Vingerling Clay* block (drainage regime as mentioned in Section 2.3), exhibited no difference in behaviour, even though T1 was performed with double the penetration rate compared with test T2. This comparison is illustrated in Figure 9.

3.2 Pile-bearing capacity

The test results for the model piles with diameters of 5.5 and 4.75 mm are shown in Figures 10 and 11, respectively. The axial load is transformed to the prototype scale. The results indicate that the bearing capacity of the PCSP is higher than the bearing capacity of the SP for both investigated model pile diameters. Piles of tests T3 and T4 were placed together in the same soil block. The results indicate that there is a difference in the absolute value of the bearing capacity between tests T2 and T3. This difference can also be seen in the measured shear strength of the clay blocks (Table 6). This illustrates that different blocks of *Vingerling Clay* do not provide reproducible conditions. The same effect is illustrated in Figure 11 where T7 and T8 were placed together in one block, and T7-repeat as well as T8-repeat were again placed together in a different block.

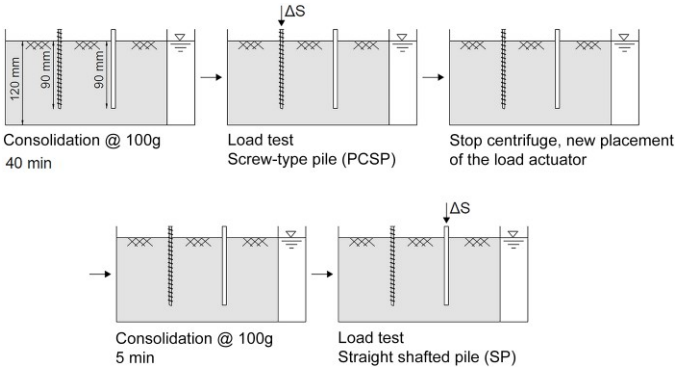

Figure 8. Centrifuge test sequence

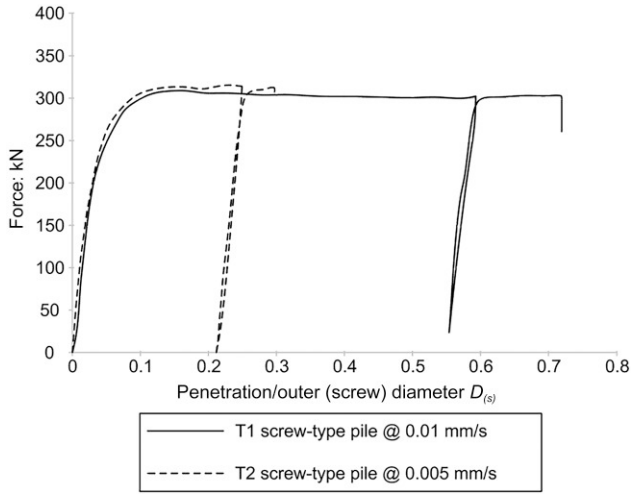

Figure 9. Model-pile test results with a diameter of 5.5 mm and different penetration rates. T1 and T2 were conducted in the same clay block

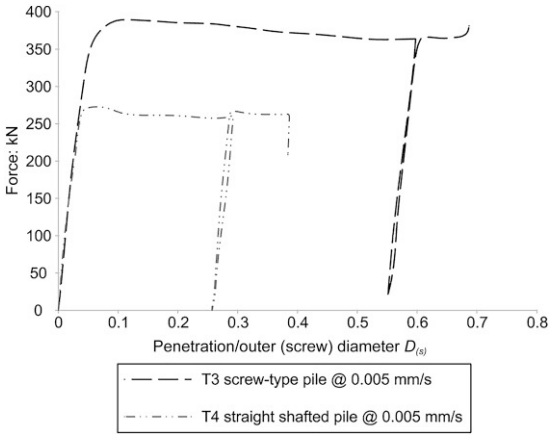

Figure 10. Model-pile test results with a diameter of 5.5 mm. T3 and T4 were conducted in the same clay block

4. Discussion

From the results given in Figure 9, it can be concluded that the loading rate is sufficiently low to assume drained material behaviour; otherwise, an influence on the bearing capacity would have been observed. Furthermore, it can be concluded that the consolidation of the clay blocks was sufficient at the onset of the test, as the tests show virtually identical behaviour, which would presumably not be the case if the clay changed its density between tests T1 and T2. The result given in Figure 9 also shows, that the pitch-matched installation of PCSP at 1*g* provides similar initial conditions for different piles.

4.1 Ultimate limit state: mobilisation of shaft friction and base resistance

As shown in the load-settlement curves, the ULS was reached for all tested piles (increase in settlements under constant load). Furthermore, it can be assumed that the bearing capacity of the piles was not influenced by the lower model boundary, as the distance between the pile tip and the model boundary was approximately 3.6 times the pile diameter after completion of the pile load test.

The mobilisation of full shaft friction is expected within the first 10 mm of settlement at prototype scale according to Figure 3 and Franke (1982). The development of shaft friction in relation to settlement is thereafter expected to remain constant. In the case of the model piles, this translates to the mobilisation of shaft friction within approximately $s/D_{(s)} = 0.02$ for both pile diameters. The mobilisation of the base resistance, in contrast, is expected to occur gradually up to a ratio of approximately $s/D_{(s)} = 0.1$.

The load-bearing behaviour of the two pile systems was identical for small pile settlements (up to approximately $s/D_{(s)} = 0.04$) and in terms of unloading and reloading hysteresis (Figures 9–11). However, a distinct difference in the way in which the ULS was reached could be observed. The SP reached a peak load (at approximately $s/D = 0.04$) without exhibiting any measurable decrease in stiffness, followed by a subsequent decrease in axial load. This compares well to the tests of Gorasia (2013), where $s/D = 0.04$ for the SP. The PCSP, however, indicated a steady increase in axial force with a gradual decrease in stiffness for $s/D_s > 0.04$.

The PCSP did not exhibit a defined peak load. A constant bearing capacity with increasing pile displacement was observed at approximately $s/D_s = 0.15$ for the 5.5 mm PCSP (Figure 10) and at $s/D_{(s)} > 0.2$ for the 4.75 mm PCSP (Figure 11). This compares well to the tests of Gorasia (2013), where $s/D_{(s)} = 0.13$ for the ribbed pile.

A comparison of the test results to the expected load-bearing behaviour of piles shows that the SP seemingly do not mobilise any significant base resistance, as no further axial load is developed for $s/D > 0.04$ (Kempfert, 2009). This observation could be ascribed to the cone-shaped tip of the pile, which is identical to the tip of the screw-type pile (Figure 5). The pile settlement at full mobilisation of the shaft friction was approximately $s/D = 0.04$ (20 mm at prototype scale) for the SP (Figure 12), resulting in a value which exceeds the recommended value given by Franke (1982) for clay soils by a factor of two. The PCSP exhibits a different loading behaviour with greater values of s/D_s than described in the literature, considering base resistance mobilisation. However, the load-settlement curves of all PCSP also indicate a constant axial load at larger pile settlements. This possibly indicates that the base

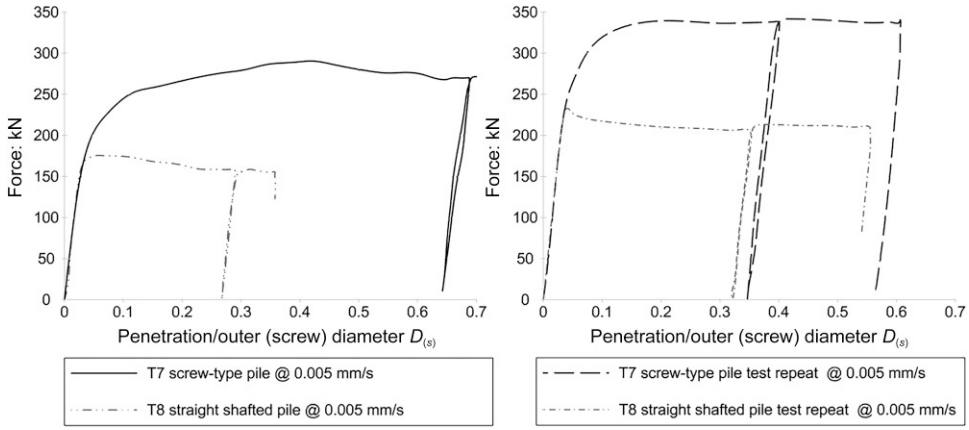

Figure 11. Model-pile test results with a diameter of 4.75 mm. T7 and T8, and T7-repeat and T8-repeat, respectively, were conducted in the same clay block

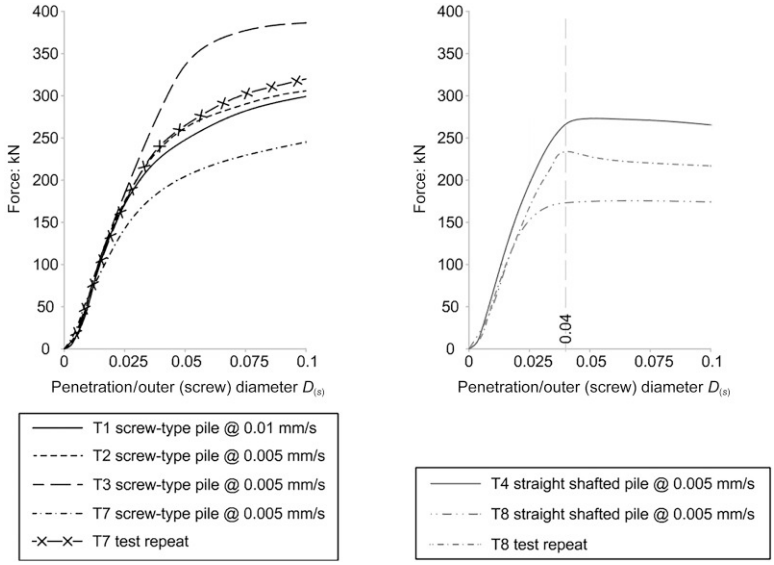

Figure 12. Load-bearing behaviour of the piles at small settlements. Axial load translated to prototype scale

resistance does not play a significant role, as the bearing capacity would increase with increasing embedment depth due to ongoing pile settlements (Kempfert, 2009).

The shaft friction was calculated as $\tau_{int} = 18.7\,\text{kN/m}^2$ according to the following approach (e.g. Knappett and Craig, 2012).

$$\tau_{int} = \beta \cdot \sigma'_{v0} \quad (4)$$

using the best fit for β after Burland (1993):

$$\beta = 0.52 \cdot \left(\frac{s_u}{\sigma'_{v0}}\right) + 0.11 \quad (5)$$

The undrained shear strength s_u was assumed to be constant ($s_{u,\text{crit}} = 27\,\text{kN/m}^2$; Table 5) as no clear s_u-profile over the height of the soil model could be estimated.

By multiplying the shaft friction τ_{int} calculated in Equation 4 with the length of the pile (an initial pile length of approximately 9 m was assumed for the prototype scale), the calculated bearing

capacity for the pile with a diameter of 0.55 m at prototype scale resulted in a value of 291 kN. The calculation for a pile with a diameter of 0.475 m at prototype scale results in a bearing capacity of 251 kN. The SP show a bearing capacity of approximately 260 kN with a diameter of 0.55 m and 150–210 kN with a diameter of 0.475 m at prototype scale. The comparison of the calculated bearing capacities of 291 kN ($D_{(s)}$ = 0.55 m) to 260 kN in the model tests or 251 kN ($D_{(s)}$ = 0.475 m) with 210 kN, respectively, indicates that (*i*) the analytical model shows reasonable results for the shaft friction under drained conditions and (*ii*) that the base resistance does not play a significant role in the load-bearing behaviour, which seems plausible regarding the pile tip shape (Figure 5).

More insight into the differences in bearing capacity of the two different pile systems may be obtained by considering the mobilised shaft friction at ULS (Table 7), as the piles showed different penetration depths at the beginning of the tests. The tip resistance was neglected, and the shaft friction was calculated as follows:

$$6. \quad q_m = \frac{Q}{(L_0 + s) \cdot D \cdot \pi}$$

The length L_0 is provided in Table 6. The ULS-Force Q is defined as the beginning of the horizontal part in the load-settlement curve (Figures 9–11), that is, constant axial load, accompanied by increasing settlements.

Comparison of tests T3 and T4 (D = 0.55 m), in which both tests were performed in the same soil model, shows a 45% higher shaft friction for the PCSP. Comparing the results of tests T7 to T8 indicates a 52% higher shaft friction for T7, and from the comparison of T7-repeat to T8-repeat, a 44% higher shaft friction could be observed in T7-repeat. It should be noted that these results are preliminary in nature, as only a small number of tests were conducted in the experimental campaign in a single soil type with a rather large scatter in absolute values of the bearing capacity. However, the results clearly exhibit the advantage of the screw-type geometry with regard to bearing capacity.

A comparison of the test results given by Meng *et al*. (2017) and by Gorasia and McNamara (2015) to the herein described tests is given in Figure 13. The results given by Gorasia and McNamara (2015) are normalised with a SP with D = 800 mm, whereas the ribbed piles (concentric ribs) have an outer diameter of D_s = 950 mm.

The graph in Figure 13 shows that for Meng *et al*. (2017), increased bearing capacity results with the presence of continuous plastic zones around the pile, whereas for larger ratios of L_p/D_s, decreased bearing capacities with discontinuous plastic zones around the pile (Figure 2) result. The tests given by Gorasia and McNamara (2015) show a similar trend. In the context of the test results given by Meng *et al*. (2017) and Gorasia and McNamara (2015), it could be argued that the herein examined PCSP geometry in terms of $L_p/D_s \approx 0.53$ is most probably close to the optimum, as the normalised bearing capacity given by Meng *et al*. (2017) and Gorasia and McNamara (2015) decreases both with a greater ratio of L_p over D_s. However, it should be noted that the bearing capacity for the PCSP at greater ratios of L_p/D_s is not described by the herein presented centrifuge tests. Moreover, the results given in Figure 13 show greater bearing capacities with increasing pile diameter ratio D_s/D.

4.2 Load-bearing behaviour and interface between pile and surrounding soil

The following discussion focuses on three aspects: (*i*) estimation of K (after pile installation); (*ii*) comparison between the theoretical estimation and physical model-test measurements of shaft friction; and (*iii*) localisation of the shear band.

i. It is reasonable to expect that the two pile systems will develop different interface characteristics with the surrounding soil, which in turn corresponds to a different load-bearing behaviour due to the different shaft geometries. This characteristic has already been mentioned by Meng *et al*. (2017), as discussed in Section 1.2.

   Neglecting any influence of base resistance, an average shaft friction for the SP of τ_{int} = 15.1 kN/m^2 can be calculated at ULS (Table 7). The mobilised shaft friction in the centrifuge

Table 7. Estimated shaft friction and bearing capacity from the centrifuge tests

Test-name	Outer pile diameter $D_{(s)}$: m	Settlement over diameter at ultimate limit state $(s/D_{(s)})_{ULS}$	Shaft friction at ultimate limit state q_m at $(s/D_{(s)})_{ULS}$: kN/m^2	Measured bearing capacity: kN	Normalised bearing capacity*
T3 (screw-type)	0.55	0.15	23.9	387	1.45
T4 (straight shafted)	0.55	0.04	16.5	267	1
T7 (screw-type)	0.475	0.2	18.6	266	1.56
T8 (straight shafted)	0.475	0.04	12.2	171	1
T7r (screw-type)	0.475	0.2	24.0	340	1.47
T8r (straight shafted)	0.475	0.04	16.7	232	1

*Compared with a straight shafted pile, tested in the same clay block

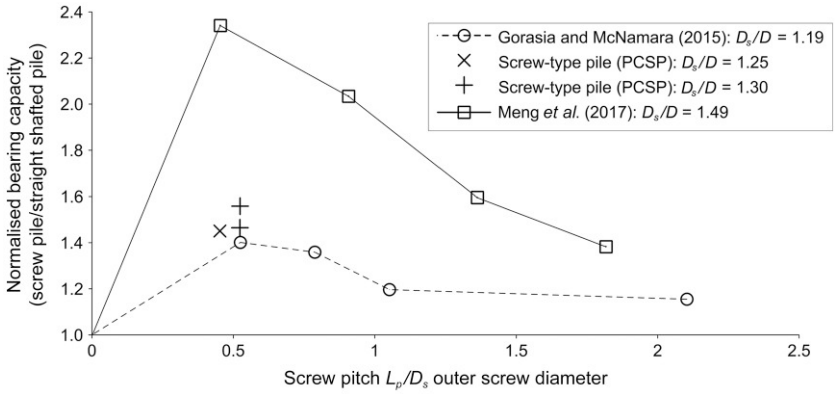

Figure 13. Comparison of normalised bearing capacity of tests given by Meng *et al*. (2017) and Gorasia and McNamara (2015)

tests is therefore lower than predicted, with $\tau_{int} = 18.7$ kPa (Equation 4) would result.

An estimate on the lateral earth pressure acting on the pile shaft can be obtained through an inverse calculation of K with σ_v' selected at half the pile height and an assumed interface friction angle $\delta' = 2/3\varphi'$:

$$K = \frac{\tau_{int}}{\sigma_v' \cdot \tan\left(\frac{2}{3}\varphi_{crit}'\right)} = 1.18 \quad (7)$$

Comparison of $K = 1.18$ with the estimated horizontal earth pressure 'at rest' ($K_0 = 0.58$) implies that the horizontal stress increased due to the installation of the displacement piles. Knappett and Craig (2012) suggested that K/K_0 for displacement piles could be as high as $K/K_0 = 2.0$.

ii. For PCSP, Equation 8

$$\tau_{int} = \sigma_h' \cdot \tan(\delta') \quad (8)$$

results in a 'shaft friction' of approximately 23.5 kN/m^2, considering the same K as was derived for the shaft friction interface with SP and considering full friction over the interface. The analytical model results in slightly higher values than the measured averaged results in the centrifuge tests ($q_{m,\text{average}} = 21$ kPa). However, the value of K cannot be derived directly from the tests conducted. The conceptual calculation of K in comparison with literature (e.g. Knappett and Craig, 2012) shows that the installation of the piles prior to the centrifuge test might play an important role in terms of more realistic values of K compared with pile prototypes. On the other hand, the results also show that the installation effects do not call into question the direct comparability of the two pile systems (SP and PCSP) in one soil model.

iii. Byrne and Houlsby (2015) presented different failure mechanisms for helical piles under tensile loading and distinguished between shaft friction and envelope friction (Section 1.2). It is feasible to distinguish between a shaft friction interface for SP and a soil friction interface for PCSP. For SP, the shear band develops between the straight pile surface and the surrounding soil. This means that the shaft friction reaches a maximum value (Figure 12; right-hand side) without any increase in strength, as is shown in the load-settlement curves by different authors. For PCSP, however, the shear band develops in the soil in the vicinity of the screw profile. In the herein presented tests, the measured shaft friction of $q_{m,\text{average}} = 21$ kN/m^2 multiplied with the cylindrical surface of the outer screw diameter, results in a load of approximately 336 kN, which is comparable with test T2 (embedded length of 9.25 m), as is illustrated in the results provided in Figure 9. It can thus be inferred that the developed shear band has a cylindrical form along the embedded length of the pile with a diameter comparable with the outer diameter of the PCSP. Knappett *et al*. (2014) and other researchers have also indicated that the shear band with axially loaded helical screw piles is supposed to develop directly at the edge of the screw blades.

5. Conclusions

The experimental campaign of centrifuge tests indicates that PCSP exhibits a higher bearing capacity in comparison with that of SP for the same outer diameter. Furthermore, a comparison of load-settlement characteristics indicates a more favourable behaviour for PCSP with continuously increasing settlements up to the maximum axial load. In contrast, SP exhibited a stiff behaviour up to the ULS with low settlement values. This was also found by Gorasia (2013).

A preliminary calculation on the interface friction of both pile systems shows that the PCSP geometry enables the development of shear bands in the soil in close proximity to the screws. The SP,

however, show shearing directly on the pile–soil interface with less friction.

The bearing capacities of the PCSP, which were reached at $s/D_s \approx 0.15$ for a pile diameter of 0.55 m and at $s/D_s \approx 0.2$ for a pile diameter of 0.475 m, were slightly higher in the clay soil used at specific conditions than the widely used ratio of $s/D \approx 0.1$. Based on the comparison of the axial compression capacity of SP with the PCSP, it may be concluded that the optimum value of L_p/D_s for PCSP is around 0.5. Furthermore, greater ratios of D_s/D also indicate an increase in bearing capacity. This could be helpful for future optimisation of pile geometries. However, the effect of installation and soil compaction on the friction interface requires further investigation.

6. Practical relevance and potential applications

The pile installation process influences the mobilised friction between the pile shaft surface and surrounding soil as well as the coefficient of lateral earth pressure along the pile. A cast-in-situ concrete pile typically exhibits a rough surface texture, which results in increased shaft friction (Atkinson, 2007). The process of drilling the hole for the placement of in situ concrete piles reduces the horizontal stresses to a further decrease due to the shrinkage of the concrete. The use of the newly developed PCSP combines many advantages:

- Screwing in the pile increases horizontal stresses in the surrounding soil and will therefore increase friction along the pile shaft.
- The helical geometry of the PCSP results in a rough soil–pile interface. Furthermore, the prefabricated piles exhibit a well-defined and stable cross-section, hence limiting the corresponding decrease in horizontal stresses.

Potential applications could be housing, nearshore foundations, or foundations in clayey soils. The advantages of PCSP outlined in this article suggest a promising potential for future practical application.

Acknowledgements

The authors are very grateful to Prof. Amin Askarinejad for his valuable contribution during the physical modelling tests and his support in the writing process of the article. The authors are also particularly grateful to J. J. de Visser, K. van Beek, and Ronald von Leeuwen, who assisted with the centrifuge tests at TU Delft. The authors would also like to thank Alphabeton AG, Switzerland and Innosuisse (Innovation cheque) for their funding of the research project and Dr Christian Spathelf for his assistance in proofreading the English article. The datasets generated and analysed in the course of the current study are available from the corresponding author upon request. This work was prepared with the assistance of generative artificial intelligence (GenAI) DeepL (https://www.deepl.com) to provide assistance in translating text elements from German into English. The entire process of using this tool was supervised, reviewed, and, when necessary, edited by the authors. The authors assume full responsibility for the content of the publication that involved the aid of GenAI.

REFERENCES

Allersma HGB (1994) The University of Delft geotechnical centrifuge. In *Centrifuge '94: Proceedings of the International Conference* (Leung CF and Lee FH (eds)). Balkema, Rotterdam, the Netherlands, pp. 47–52.

Arnold A and Askarinejad A (2020) Behaviour of prefabricated concrete screw piles under axial loading. In *Proceedings of the 4th European Conference on Physical Modelling in Geotechnics* (Jan Laue, Tarun Bansal (eds)), Lulea University of Technology, Sweden, pp. 287–288.

Arnold A, Espinosa T, Felder H-P, Zuercher E and Askarinejad A (2021) Seilbahnstützen-Fundamente für die ZüriBahn, *35. Christian Veder Kolloquium*, Technische Universität Graz.

Atkinson J (2007) *The Mechanics of Soils and Foundations* Second edition. Taylor & Francis, New York, NY, USA.

Burland J (1993) Closing address. In *Proceedings of Recent Large-Scale Fully Instrumented Pile Tests in Clay. Institute of Civil Engineers*. London. pp. 590–595.

Byrne BW and Houlsby GT (2015) Helical piles: an innovative foundation design option for offshore wind turbines. *Philosophical Transactions. Series A, Mathematical, Physical, and Engineering Sciences* **373**: 20140081, 10.1098/rsta.2014.0081.

Cerfontaine B, Brown MJ, Knappett JA *et al.* (2021) Control of screw pile installation to optimise performance for offshore energy applications. *Géotechnique* **73(3)**: 234–249, 10.1680/jgeot.21.00118.

Davidson C, Brown MJ, Cerfontaine B *et al.* (2022) Physical modelling to demonstrate the feasibility of screw piles for offshore jacket-supported wind energy structures. *Géotechnique* **72(2)**: 108–126, 10.1680/jgeot.18.P.311.

Fioravante V (2002) On the shaft friction modelling of non-displacement piles in sand. *Soils and Foundations* **42(2)**: 23–33, 10.3208/sandf.42.2_23.

Franke E (1982) Pfähle. In *Grundbautaschenbuch Teil 2* (3rd. ed.). Ernst & Sohn Verlag für Architektur und technische Wissenschaften GmbH & Co. KG, Berlin.

Garnier J, Gaudin C, Springman SM *et al.* (2007) Catalogue of scaling laws and similitude questions in geotechnical centrifuge modelling. *International Journal of Physical Modelling in Geotechnics* **7(3)**: 1–23, 10.13140/2.1.1615.3281.

Gorasia RJ (2013) *Behaviour of ribbed piles in clay*. Doctoral Thesis, City University, London.

Gorasia RJ and McNamara A (2015) High-capacity ribbed pile foundations. *Proceedings of the Institution of Civil Engineers Geotechnical Engineering* **169(3)**: 264–275, 10.1680/jgeen.15.00073.

Hiemstra JF and Rijsdijk KF (2003) Observing artificially induced strain: Implications for subglacial deformation. *Journal of Quaternary Science* **18(5)**: 373–383, 10.1002/jqs.769.

Hird CC and Stanier SA (2010) Modelling helical screw piles in clay using a transparent soil. In *Proceedings of the 7th International Conference on Physical Modelling in Geotechnics*, Taylor & Francis Group, London. pp. 769–774.

Jardine RJ, Zhu BT, Foray P and Yang ZX (2013) Measurement of stresses around closed-ended displacement piles in sand. *Géotechnique* **63(1)**: 1–17, 10.1680/geot.9.P.137.

Kempfert H-G (2009) Pfahlgründungen. In *Grundbautaschenbuch Teil 3*. Ernst & Sohn Verlag für Architektur und technische Wissenschaften GmbH & Co. KG, Berlin, pp. 73–277.

Knappett J and Craig R (2012) *Craig's Soil Mechanics* (8th. ed.). Spon Press, Oxon.

Knappett JA, Brown MJ, Brennan AJ and Hamilton L (2014) Optimising the compressive behaviour of screw piles in sand for marine renewable energy applications, *International Conference on Piling & Deep Foundations*, Stockholm, Sweden.

Kutter BL (1994) Recent advances in centrifuge modeling of seismic shaking. State-of-the-Art Paper, In *Proceedings, 3rd International Conference on Recent Advances in Geotechnical Earthquake Engineering and Soil Dynamics*, Vol. 2, pp. 927–942.

Lambe TW and Whitman RV (1969) *Soil Mechanics*. John Wiley & Sons, Inc.

Lang H-J, Huder J, Amann P and Puzrin AM (2011) *Bodenmechanik Und Grundbau*. Springer, Berlin Heidelberg.

Lehane BM, Jardine RJ, Bond AJ and Frank R (1993) Mechanisms of shaft friction in sand from instrumented pile tests. *Journal of Geotechnical Engineering* **119(1)**: 19–35, 10.1061/(ASCE)0733-9410(1993)119:1(19).

Li Q, Prendergast LJ, Askarinejad A, Chortis G and Gavin K (2020) Centrifuge modeling of the impact of local and global scour erosion on the monotonic lateral response of a monopile in sand. *Geotechnical Testing Journal* **43(5)**: 1084–1100, 10.1520/GTJ20180322.

Madabhushi G (2014) *Centrifuge Modelling for Civil Engineers*. CRC Press, Boca Raton, FL, USA.

Meng Z, Chen J-J and Wang JH (2017) Numerical analysis of bearing capacity of drilled displacement piles with a screw-shaped shaft in sand. *Marine Georesources & Geotechnology* **35(5)**: 661–669, 10.1080/1064119X.2016.1213777.

Nabizadeh F and Choobbasti AJ (2017) Field study of capacity helical piles in sand and silty clay. *Transportation Infrastructure Geotechnology* **4(1)**: 3–17, 10.1007/s40515-016-0036-0.

O'Rourke T and Kulhawy FH (1984) Observations on load tests for drilled shafts. In *Proc. Drilled Piers and Caissons II*. ASCE, Reston, VA, pp. 113–128.

Randolph MF, Cassidy MJ, Gourvenec SM and Erbrich C (2005) Challenges of offshore geotechnical engineering. In *Proceedings 16th International Conference of Soil Mechanics and Foundation Engineering*, Osaka, Japan, Vol. 1, pp. 123–176.

Terzaghi K (1943) *Theoretical Soil Mechanics*. Wiley and Sons.

Tolun M, Emirler B, Ertugrul OL and Yildiz A (2023) Effect of surface roughness characteristics on the uplift capacity of piles: a physical modelling study. *Marine Georesources & Geotechnology* **41(8)**: 935–947, 10.1080/1064119X.2022.2110025.

Vermeer PA and Meier CP (1998) *Standsicherheit Und Verformungen Bei Tiefen Baugruben in Bindigen Böden*. Vorträge Der Baugrundtagung in Stuttgart, pp. 133–148.

Wehnert M (2006) *Ein Beitrag Zur Drainierten Und Undrainierten Analyse in Der Geotechnik*. Universität Stuttgart.

Wood DM (2004) *Geotechnical Modelling*. CRC Press. London, 10.1201/9781315273556.